

## MODELLING OF THE ELECTRON DISTRIBUTION BASED ON BREMSSTRAHLUNG EMISSION DURING LOWER-HYBRID CURRENT DRIVE ON PLT

J. STEVENS, S. VON GOELER, S. BERNABEL, M. BITTER,  
T.K. CHU, P. EFTHIMION, N. FISCH, W. HOOKE, J. HOSEA,  
F. JOBES, C. KARNEY, E. MESERVEY, R. MOTLEY, G. TAYLOR  
Princeton Plasma Physics Laboratory,  
Princeton University,  
Princeton, New Jersey,  
United States of America

**ABSTRACT.** Lower-hybrid current drive requires the generation of a high-energy electron tail anisotropic in velocity. Measurements of bremsstrahlung emission produced by this tail are compared with the calculated emission from reasonable model distributions. The physical basis and the sensitivity of this modelling process are described, and the plasma properties of current-driven discharges which can be derived from the model are discussed.

### 1. INTRODUCTION

During lower-hybrid current drive an energetic current-carrying electron tail is created by the unidirectional RF waves. One of the primary goals of the Princeton Large Torus (PLT) lower-hybrid experiment [1–5] is to determine the velocity distribution of this tail. A method for diagnosing the high-energy electron velocity distribution is to measure the bremsstrahlung produced by those electrons [6–8]. Several difficulties must be overcome in order to utilize the bremsstrahlung method. First, since the electron distribution during current drive is expected to be anisotropic, it is necessary to measure the bremsstrahlung as a function of angle to the magnetic field in order to gain information about the degree of anisotropy of the electron distribution. The second difficulty with the bremsstrahlung technique is that the photon energy distribution measured by a pulse-height-analysis system is not the electron energy distribution. In fact, photons of a given direction and energy ( $h\nu$ ) can result from any electron with arbitrary direction and with kinetic energy higher than  $h\nu$ . Because of these difficulties, it is practically impossible to derive the electron distribution directly from the bremsstrahlung data. Instead, one must assume a relatively simple model for the electron distribution and determine its consistency with the data. The parameters of the model which best fit the data are obtained by iteration.

The resultant model distribution is obviously not unique, but it is able to describe many of the essential features of the true electron distribution. Higher-order features can be added to the model as long as their effect on the bremsstrahlung emission can be distinguished by comparison with the data.

The accompanying paper [9] describes how the bremsstrahlung measurements are made and how the electron distribution function behaves for various plasma and RF conditions. The modelling calculations are described in Section 2 of this paper, and fits from increasingly refined models are compared to the data in Section 3. A spatially homogeneous, three-temperature model is fit to the data in Section 3.1, and the sensitivity of that fit to the model temperatures is discussed in Section 3.2. More complicated models in velocity space and physical space are discussed in Sections 3.3 and 3.4, with the result that the best overall fit to the data involves a model which is spatially inhomogeneous as well as anisotropic. Section 4 is a discussion of the distribution function calculated directly from the Fokker-Planck equation with a quasi-linear RF diffusion term. For reasonable parameters, the Fokker-Planck quasi-linear RF theory gives a good fit to the bremsstrahlung data. Finally, the implications of the modelling results to current drive plasmas are discussed in Section 5.

2. SOLUTION PROCEDURE

2.1. Experimental data

Measurements of hard X-rays as a function of energy and angle were made on the PLT tokamak with the experimental arrangement [4] shown schematically in Fig. 1. The PLT plasma has a major radius of 1.32 m and a minor radius of 0.4 m. A 3 in. × 3 in. NaI (TI) detector views the plasma along a line-of-sight determined by two apertures with angular resolution of about 1°. The detector line-of-sight intersects the magnetic axis of the plasma at an angle defined as  $\theta$ . The detector apparatus can be pivoted so as to allow  $\theta$  to vary between 28° and 86°. The range of  $\theta$  is increased to 28°–152° by reversing the direction of all fields and currents in PLT as well as the phasing of the lower-hybrid waveguides.

This paper will discuss in detail a single set of measurements as a function of  $\theta$  in order to illustrate the modelling procedure. The X-ray data were taken in a plasma with a current of 180 kA, a line average density  $\bar{n}_e = 5 \times 10^{12} \text{ cm}^{-3}$ , and an 800 MHz RF power of 200 kW. The RF power which maintained this discharge was launched primarily in one toroidal direction by a six-element waveguide grill with a relative phasing of 90° between guides. The RF power spectrum was peaked at  $n_{\parallel} \approx 2.25$  with a width at half maximum of  $\Delta n_{\parallel} \approx 1.5$ . The measurement of bremsstrahlung emission versus energy and angle for this discharge is shown in Fig. 2b. The symbols in the figure show photon counts per 3 keV energy interval at four different photon energies and fourteen different viewing angles. Data at each viewing angle are the sum over five plasma shots with the RF on for 0.35 s each shot. The data have been weighted to account for the

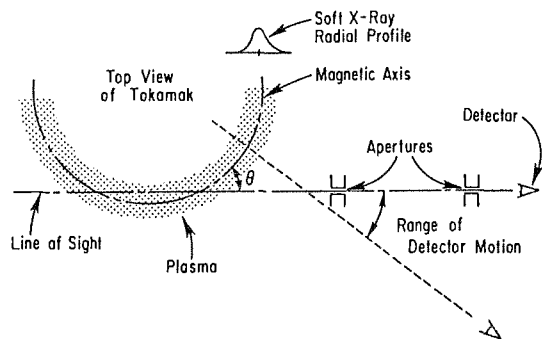


FIG. 1. Schematic diagram of experimental geometry. Angle between magnetic axis and detector line-of-sight,  $\theta$ , can be varied between extremes of 28° to 86°.

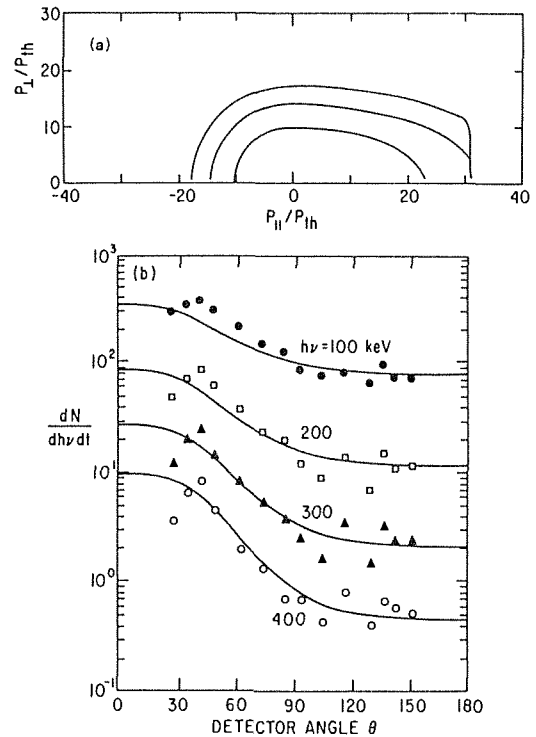


FIG. 2. (a) Model distribution function plotted versus  $p_{\parallel}/p_{th}$  and  $p_{\perp}/p_{th}$ , where 1 keV thermal bulk plasma is assumed. Every contour represents factor of 2. Contours for thermal part of distribution are not shown. (b) Photon counts per 3 keV energy bin and 2.8 s time interval versus detector viewing angle  $\theta$ . Symbols are measured data for photon energies of 100, 200, 300, and 400 keV. Solid lines are computed from model distribution shown in (a).

different lengths of the line-of-sight through the plasma at each viewing angle. These weighting factors are computed from radial profiles determined by Abel inversion of 14 keV radial chord X-ray measurements which are made separately with a Si(Li) detector [10]. It is assumed, for lack of better information, that the fast-electron tail has the same radial density profile as that determined from 14 keV soft X-rays. The radial profile for these data is shown in the accompanying paper [9].

The statistical counting errors are approximately 10% for most of these data but increase for energies above about 300 keV, because of limited statistics. Some improvement in the counting statistics can be made by averaging over adjacent 3 keV energy channels. Background counts, which can come from the limiter or elsewhere, constitute a further source of error for the higher-energy photons ( $h\nu > 300 \text{ keV}$ ). A more serious and difficult-to-estimate source of error is the shot-to-shot variation during the 80 plasma discharges

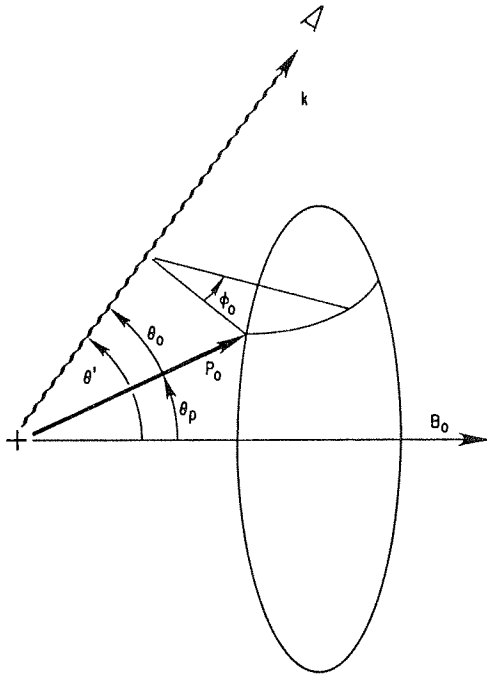


FIG.3. Geometry of bremsstrahlung emission process at any position in plasma. Directions of external magnetic field  $B_0$ , incident electron momentum  $p_0$ , and emitted photon  $k'$  are shown.

needed to construct Fig.2b. It will be shown that angular resolution better than about  $40^\circ$  in  $\theta$  is not expected, so that the smoothness of the photon count data versus  $\theta$  gives perhaps the best indication of the shot-to-shot variation of conditions. Figure 2b shows that for  $90^\circ \lesssim \theta \lesssim 150^\circ$  the jitter in the data can be as much as  $\pm 15\%$  at  $h\nu = 100$  keV and  $\pm 50\%$  at  $h\nu = 300$  keV. Another difficult source of error to identify is the effect of small electric fields on the high-energy electron tail. A loop voltage of less than 50 mV is enough to cause 500 keV electrons in the RF-produced tail to run away in these discharges. Since it is desired to measure the tail created by the RF alone, all the tokamak magnetics quantities (plasma current, internal inductance, and Ohmic-heating transformer current) were held as constant as possible to minimize residual voltages.

There are two main features of the data that the modelling should reproduce. One is the asymmetry in the X-ray emission between small and large viewing angles. Figure 2b shows that there are approximately four times more counts for 100 keV photons and approximately ten times more counts for 400 keV photons at  $\theta = 28^\circ$  as compared with  $\theta = 152^\circ$ . The

second main feature of the data that the model should reproduce is the slope of the plot of photon counts versus photon energy at each viewing angle.

## 2.2. Bremsstrahlung emission

The calculation for the number of photons emitted in a given energy and time interval and at a given viewing angle proceeds straightforwardly by integrating the bremsstrahlung cross-section over the distribution of electron momenta. For any local point in the plasma (Fig.3):

$$\frac{dN(k', \theta')}{dk' dt} \propto \int d^3 \vec{p}_0 f(\vec{p}_0, \theta_p) \frac{d\sigma(k', \theta_0, p_0, Z_i)}{dk' d\theta_0} v_0 \quad (1)$$

where  $k' \equiv h\nu/mc^2$  is the photon energy normalized to  $mc^2$ ,  $p_0$  is the momentum of the incident electron normalized to  $mc$ ,  $v_0$  is the velocity of the incident electron,  $\theta_0$  is the angle between  $\vec{p}_0$  and  $\vec{k}'$ ,  $\theta_p$  is the angle between the external magnetic field  $\vec{B}_0$  and  $\vec{p}_0$ , and  $\theta'$  is the angle between  $\vec{B}_0$  and the emitted photon  $\vec{k}'$ . The bremsstrahlung cross-section, differential in energy and angle, is  $d\sigma/dk d\theta_0$ . The tail electron distribution function  $f$  is the unknown which we wish to find. Summing the emission along the detector line-of-sight gives the number of photons seen by the detector at a given energy and viewing angle:

$$\begin{aligned} N(k, \theta) &= \frac{A_1 A_2}{4\pi b^2} \int_{\Delta t} dt \int_{\Delta k} dk' G(k, k') \\ &\times \int d\ell W(\theta, \theta', \ell) n_e(\ell) n_t(\ell) \int_{k'+1}^{\infty} dp_0 c p_0^3 / E_0 \\ &\times \int_0^\pi \sin(\theta_0) d\theta_0 \left( Z_{\text{eff}} \frac{d\sigma_{ei}}{dk' d\theta_0} + \frac{d\sigma_{ee}}{dk' d\theta_0} \right. \\ &\left. + \sum_i \left( \frac{n_i}{n_e} \right) \frac{d\sigma_{ri}}{dk' d\theta_0} \right) \int_0^{2\pi} d\phi_0 f(p_0, \theta_p, \ell) \quad (2) \end{aligned}$$

where the relations  $\int d^3 \vec{p}_0 f = 1$ ,  $v_0/c = p_0/E_0$ ,  $E_0^2 = p_0^2 + 1$ , and  $\theta_p = \cos^{-1} [\cos \theta' \cos \theta_0]$

$+\sin\theta'\sin\theta_0\cos\phi_0]$  are used for evaluating the integrals. In Eq.(2), the quantity  $G(k, k')$  represents the response of the pulse height system,  $k$ , to an incident photon of energy  $k'$ . The photo peak response of the 3 in.  $\times$  3 in. NaI crystal is practically 100% for energies in the 30 up to 400 keV range, and the energy resolution is approximately 6.5% at  $k = 662$  keV and varies as  $k^{-1/2}$  [11]. Therefore, since energy resolution better than this is of no immediate interest, it is a good approximation to take  $G(k, k') \cong \delta(k, k')$ .

The function  $W(\theta, \theta', \varrho)$  takes into account the fact that each external viewing angle  $\theta$  views a different path length through the plasma and also that each external viewing angle  $\theta$  actually samples many different local angles of emission,  $\theta'$ , along the line of sight. The plasma bulk electron density  $n_e$ , the density of tail electrons  $n_t$ , and the tail distribution function  $f$  can all vary along the line-of-sight. The quantities  $A_1$  and  $A_2$  are the areas of the detector apertures, and  $b$  is the spacing between apertures. Finally, the bremsstrahlung cross-section is divided into several contributions described below.

2.3. Bremsstrahlung cross-sections

X-ray photons in the energy range of the NaI detector (30–750 keV) are produced in the plasma by electron-ion bremsstrahlung, electron-electron bremsstrahlung, or by electron-ion recombination radiation. A relativistic Born approximation formula for electron-ion bremsstrahlung is given by Gluckstern and Hull [12–14]. In addition, this cross-section is multiplied by a Coulomb correction factor derived by Elwert [15] which improves the result, especially for photon energies comparable to the incident electron energy. The Born-Elwert cross-section, differential in both photon energy and angle, differs from more accurate calculations by less than 10% for most emission angles in the 50–500 keV range for low-Z ions [16–18]. The largest discrepancy occurs at angles  $\theta_0$  at which the emission is smallest. This is satisfactory for the present data which have at least 10% error. Polar plots of the electron-ion bremsstrahlung intensity versus emission angle are shown in Fig.4a for 50 keV and 500 keV incident electrons. It is the forward peaking of the bremsstrahlung emission which makes it possible to transform from X-ray spectra to electron energy spectra. However, the difficulty of this deduction process is also apparent from the figure since electrons of a single energy and direction can emit photons at all energies below the kinetic energy of the electron  $T_0 (\equiv E_0 - 1)$  and in all directions. The angular width of the forward

peak is approximately  $40^\circ$  at  $h\nu = 500$  keV which is indicative of the smallest angular resolution in velocity space that can be achieved by bremsstrahlung measurements.

The relativistic Born approximation formula given by Haug is used for computing electron-electron bremsstrahlung [19]. This formula again is multiplied by an Elwert-Coulomb correction factor. The target electrons are assumed here to be stationary. In general, the contribution from electron-electron bremsstrahlung is comparable to the electron-ion term for electrons with normalized kinetic energy  $T_0 > 1$  (511 keV) in plasmas with  $Z_{eff} = 1$  [20–21]. For most electron distributions of interest here, where  $Z_{eff} > 1$  and  $T_0 < 1$ , the electron-electron term contributes less than 10% to the total emission. Polar plots of the electron-electron bremsstrahlung intensity versus emission angle are shown in Fig.4b for 50 keV and 500 keV incident electrons and stationary target electrons.

A third possible mechanism for plasma X-ray emission is recombination radiation. The ratio of

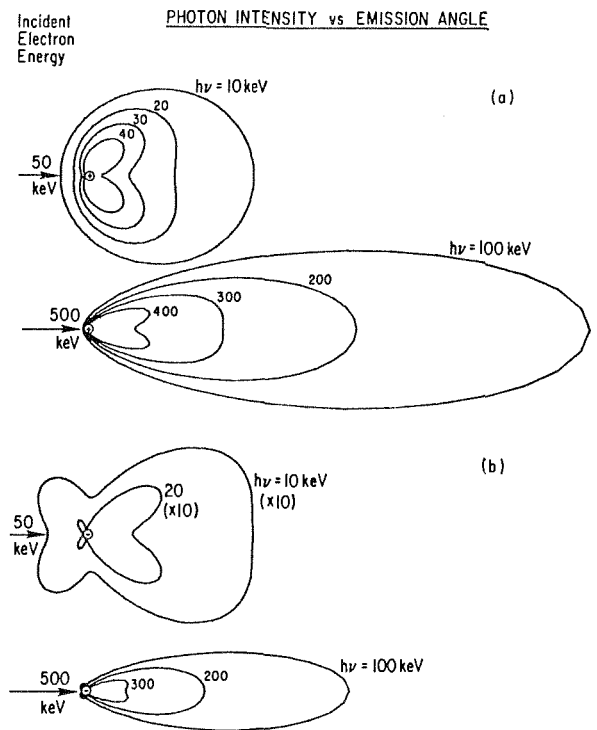


FIG.4. Polar plot of bremsstrahlung intensity for 50 and 500 keV incident electrons colliding with (a) protons and (b) electrons. Intensity patterns are plotted for photon energies equal to every 20% of incident electron energy. Case of 50 keV electrons colliding with electrons is plotted on expanded scale.

total recombination radiation to bremsstrahlung can be estimated from non-relativistic formulas [22, 23]. However, relativistic effects as well as the angular dependence of recombination emission may modify these estimates. It is known, for example, that the cross-section for the photo effect (inverse process of recombination emission) falls less steeply with  $k$  at relativistic energies [13]. To estimate the contribution of recombination radiation, a relativistic Born approximation cross-section was obtained for K-shell recombination radiation from the corresponding K-shell photo-effect cross-section by a detailed balance argument:

$$\sigma_{\text{recomb}} = \frac{c}{v} \frac{\rho_k}{\rho_e} \sigma_{\text{photo}} = \frac{k^2}{p^2} \sigma_{\text{photo}} \quad (3)$$

where  $\rho_k, \rho_e$  are the densities of quantum states for the emitted recombination photon and the photo-effect electron, respectively. The relativistic Born approximation cross-section for K-shell photo-emission,  $\sigma_{\text{photo}}$ , is given by Sauter [24]. The cross-section is multiplied by a 'rule-of-thumb' factor of 1.25 to account for recombination into other energy shells [13]. Results using this cross-section indicate that recombination radiation is negligible compared to electron-ion bremsstrahlung (< 5%) at all viewing angles for photon energies between 50 and 400 keV and for both light impurity ions (C, O) as well as heavier ions (Fe, Ti, Cr, Ni) in He-like states. This assumes an electron tail temperature higher than 100 keV. Therefore, recombination radiation will be neglected in the rest of this paper. Recombination radiation from the RF-produced tail could become significant for tail temperatures lower than 100 keV or for discharges with higher bulk temperatures where fully stripped heavy impurities make a large contribution to  $Z_{\text{eff}}$ .

#### 2.4. Model electron distributions

A description of the tail electron-distribution function which fits the data is built up step by step by assuming a simple model and then adding additional features as long as they can be justified by the data. A simple model which can display velocity space anisotropy is given by

$$f(\vec{p}) = C_N \exp\left(-\frac{p_{\perp}^2}{2T_{\perp}} - \frac{p_{\parallel}^2}{2T_{\parallel F}}\right) \text{ for } p_{\parallel} \geq 0$$

$$= C_N \exp\left(-\frac{p_{\perp}^2}{2T_{\perp}} - \frac{p_{\parallel}^2}{2T_{\parallel B}}\right) \text{ for } p_{\parallel} < 0 \quad (4)$$

$$= 0 \quad \text{for } p_{\parallel}, p_{\perp} > p^*$$

where  $f(\vec{p})$  is assumed to be spatially uniform throughout the plasma. The constant  $C_N$  is chosen to satisfy the condition

$$\int d^3 p f(\vec{p}) = 1$$

The momenta are again normalized to  $mc$  and the temperatures are normalized to  $mc^2$ . This three-temperature model reduces to a bi-Maxwellian when  $T_{\parallel F} = T_{\parallel B}$  and  $T_{\perp}, T_{\parallel} \ll 1$ . The four adjustable parameters available to fit the data are:  $T_{\parallel F}$  (forward parallel temperature),  $T_{\perp}$  (perpendicular temperature),  $T_{\parallel B}$  (backward parallel temperature), and  $p^* = (E^{*2} - 1)^{1/2}$  (maximum momentum). Note that the forward direction ( $p_{\parallel} > 0$ ) corresponds to the direction of the wave phase velocity. It will be shown in Section 3.3 that allowing additional freedom in momentum space for  $f(\vec{p})$  cannot be justified by the present data. However, allowing  $f(\vec{p})$  to vary with plasma minor radius appears to be able to explain an essential feature of the data (Section 3.4).

An alternative to assuming a model distribution function is to calculate the electron distribution using the Fokker-Planck equation with an added quasi-linear term [25, 26]. The adjustable parameters are the minimum and maximum extent of the RF wave spectrum ( $W_1$  and  $W_2$ ), the strength of the RF diffusion coefficient  $D_{QL}(W)$ , and  $Z_{\text{eff}}$  of the plasma. The comparison of the calculated bremsstrahlung emission with the data proceeds in the same manner as for the three-temperature model. The resultant distribution functions for both models should be very similar. The results of comparing the quasi-linear, Fokker-Planck calculation with the data are discussed in Section 4.

#### 2.5. Fitting criteria

Obtaining a best fit of the model parameters to the data proceeds by assuming values for the adjustable parameters, calculating the bremsstrahlung as a function of energy and angle, and then applying a statistical test to measure the quality of fit. A least-squares fitting criterion was used to minimize the mean percent

difference,  $\epsilon$ , between the measured photon counts and calculated photon counts with all data points weighted equally ( $J$  = number of points):

$$\epsilon = \{ \exp(\sqrt{\delta^2/J}) - 1 \} \times 100\% \quad (5)$$

where

$$\delta^2 = \sum_{j=1}^J \{ \ln(N_j^D(k, \theta)) - \ln(N_j^C(k, \theta)) \}^2 \quad (6)$$

$N_j^D$  is the measured number of photon counts, and  $N_j^C$  is the calculated number of photon counts at photon energy  $k$  and detector angle  $\theta$ .

A  $\chi^2$ -test to estimate the correctness of the fit is not very meaningful because of the difficulty of estimating the experimental and computational errors for this experiment. In addition to the usual counting statistics which are  $\lesssim 10\%$ , there are possibly shot-to-shot differences in the plasma discharges, varying levels of background X-rays at each viewing angle, and perhaps small alignment errors. There are  $\lesssim 10\%$  uncertainties in the bremsstrahlung cross-sections, as well. Fits with  $\epsilon \approx 25\%$  have been obtained, which are probably indicative of the overall uncertainty.

### 3. COMPARISON WITH EXPERIMENTAL DATA

#### 3.1. Homogeneous distribution function

As a first approximation it was assumed that the tail distribution function was homogeneous, i.e. that it was the same everywhere in the plasma. The solid lines in Fig.2b are a fit to the data for photon energies of 100, 200, 300, and 400 keV, assuming a three-temperature distribution function with the parameters  $T_{\parallel F} = 750$  keV,  $T_{\perp} = 150$  keV,  $T_{\parallel B} = 150$  keV, and the maximum kinetic energy  $mc^2(E^* - 1) = 600$  keV. These parameters give a mean square percent difference of  $\epsilon \approx 32\%$  between the calculated and the measured photon counts. A contour plot of the model electron distribution is shown in Fig.2a. Note that the model distribution has an enhanced forward temperature, i.e. in the direction of the wave phase velocity. The bremsstrahlung spectrum calculated from the model duplicates the two main features of the data: (1) the general peaking of the emission for forward viewing angles ( $\theta \lesssim 90^\circ$ ) and (2) the relative spacing between

lines with 100 keV increments in photon energy (i.e. the slope of the X-ray spectrum at each viewing angle).

A major discrepancy between the data and the calculation from the model is the relatively narrow emission peak in the data at  $\theta \cong 45^\circ$  and the subsequent fall off as  $\theta$  approaches  $28^\circ$ . The peak is most pronounced for high photon energy ( $h\nu \approx 400$  keV). A smaller peak occurred in other data sets. The peak was always present during the RF pulse and always disappeared after the RF turnoff. The presence of this peak indicates that during current drive the distribution is more complicated than first assumed. More refined models such as allowing  $f(\vec{p})$  to vary with minor radius will be investigated in later sections.

The cutoff energy  $E^*$  was introduced as a fourth free parameter for the model distribution.  $E^*$  can be used to simulate a high-energy limit to the distribution function which could result from a maximum wave phase velocity due to the lower hybrid wave accessibility condition. However, it is not possible with the present data to distinguish between models with and without a cutoff energy  $E^*$ . A best fit, for  $E^* \rightarrow \infty$ , is obtained with  $T_{\parallel F} = 450$  keV,  $T_{\perp} = T_{\parallel B} = 150$  keV. This gives a mean square difference between model and data of  $\epsilon = 42\%$ , which is slightly worse than for the model with  $mc^2(E^* - 1) = 600$  keV and  $T_{\parallel F} = 750$  keV. In either case, the tail distribution function is greatly enhanced in the direction of the wave phase velocity. Data for photon energies  $h\nu > 500$  keV would be necessary to distinguish between the case of a cutoff in the forward distribution and the case of a distribution which tails off more gradually at high energies.

#### 3.2. Sensitivity of the calculated emission to the model parameters

A critical question for the modelling is the sensitivity of the calculated X-ray spectra to the model parameters. Figure 5 is a plot of calculated bremsstrahlung angular distributions at  $h\nu = 100$  and 300 keV for the best fitting model distribution given in the previous section (solid lines) along with spectra which are calculated as one parameter at a time is varied by  $\pm 50\%$  (dotted lines). It is apparent from Fig.5 that the major change in the X-ray emission intensity occurs at the angles for which the electron distribution has changed, i.e. if  $T_{\perp}$  is varied, then the major change in X-ray emission occurs between  $\theta = 60^\circ$  and  $\theta = 120^\circ$ . Similarly, variations in  $T_{\parallel F}$  affect primarily the forward X-ray emission ( $\theta \lesssim 60^\circ$ ) and variations in  $T_{\parallel B}$  affect mainly the backward X-ray emission ( $\theta \gtrsim 120^\circ$ ).

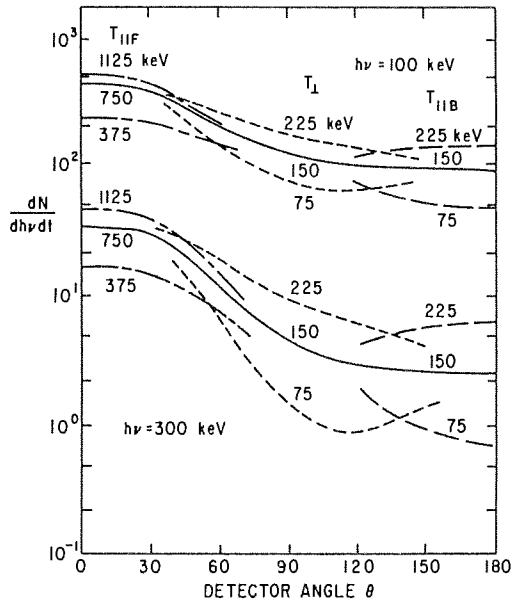


FIG.5. Calculated photon counts versus  $\theta$  for  $h\nu = 100$  and  $300$  keV. Solid lines are best fit to data. Various dashed lines represent a  $\pm 50\%$  change in one model parameter with other parameters maintaining their best fit values.

This is to be expected because the X-ray emission patterns are peaked strongly in the direction of the incident electron velocities (Fig.4).

The slopes of the photon spectra are not very sensitive to the tail electron temperature. For example, a change in  $T_{\perp}$  of 50% changes the perpendicular photon slope  $\{T_{ph} \equiv -\Delta(h\nu)/\Delta \ln(N)\}$  by less than 16%. The slope of the photon spectrum becomes even less sensitive to electron temperature for electron temperatures above 150 keV. However, the determination of tail temperature is improved somewhat by having fourteen different viewing angles at which the slopes are compared with the data.

Many X-ray emission experiments in tokamaks are carried out at  $\theta = 90^\circ$ . However, the  $90^\circ$  emission alone can be very insensitive to the energetic parallel component of distributions such as those encountered in runaway discharges or in current drive discharges. A plot of the calculated  $90^\circ$  photon temperature versus forward temperature is given in Fig.6, with  $T_{\perp}$  and  $T_{\parallel B}$  taking on selected values. The figure shows that large changes in  $T_{\parallel F}$  have only a slight effect on the slope of the  $90^\circ$  bremsstrahlung spectrum when  $T_{\parallel F} > T_{\perp}$ . The parallel temperature,  $T_{\parallel F}$ , has no effect on the  $90^\circ$  photon temperature when  $T_{\parallel F} < T_{\perp}$ . These calculations indicate that it is necessary to interpret fixed-angle X-ray measurements

with caution when dealing with anisotropic electron distributions.

### 3.3. Additional velocity space structure

The problem of the data peaking at  $\theta \approx 45^\circ$  in Fig.2b could not be accounted for by a simple, homogeneous, three-temperature distribution. A test was made to determine whether the peak at  $\theta \approx 45^\circ$  could be the result of a finer structure in velocity space. An obvious choice is a distribution with electrons only at  $\theta_p = 45^\circ$  in velocity space. The X-ray emission from such a 'cone' distribution with  $T = 300$  keV is shown in Fig.7. The bremsstrahlung calculated from this 'cone' distribution has an emission peak at  $h\nu = 400$  keV and  $\theta \sim 45^\circ$  which has a width  $\Delta\theta \approx 40^\circ$  at half maximum. This is approximately twice as wide as the peak in the data, and in fact, the calculated peak represents the minimum angular resolution obtainable by bremsstrahlung measurements at these energies. Furthermore, this 'cone' distribution is unphysical in a tokamak where it is expected that collisions would broaden such narrow angular distributions. Therefore, the narrow peaking of the data at emission angles near  $\theta \approx 45^\circ$  is not primarily a velocity space feature of the distribution function.

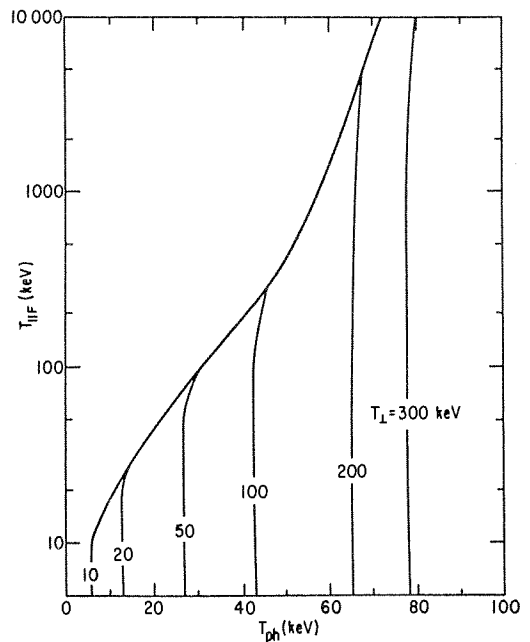


FIG.6. Perpendicular photon temperature versus forward parallel temperature for  $T_{\perp} = T_{\parallel B} = 10, 20, 50, 100, 200,$  and  $300$  keV. Photon temperature,  $T_{ph} \equiv \Delta k/\ln[N(k)/N(k+\Delta k)]$  is evaluated at  $k = 200$  keV and  $\theta = 90^\circ$ .

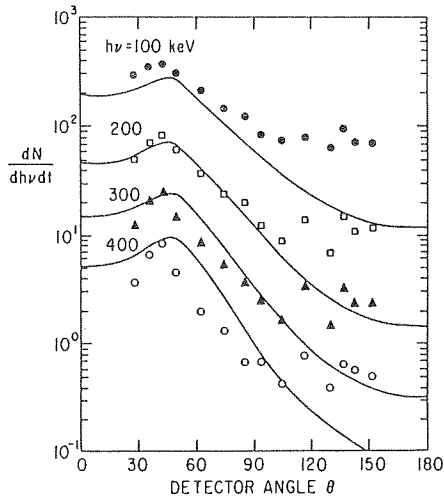


FIG. 7. Bremsstrahlung emission versus  $\theta$  calculated from model distribution given by  $f \propto \delta(\theta_p - 45^\circ) \exp(-p^2/2T)$ , where  $T = 300 \text{ keV}/mc^2$ . Even though electrons are modelled to be at single angle in velocity space, calculated emission peak for  $h\nu = 400 \text{ keV}$  at  $\theta = 45^\circ$  is broader than peak in data.

### 3.4. Inhomogeneous distribution function

The electron distribution function may also be a function of radius. The fit to the bremsstrahlung data in Fig.8 assumes a two-step radial variation with the following parameters:

Radius	$T_{\parallel F}$ (keV)	$T_{\perp}$ (keV)	$T_{\parallel B}$ (keV)	$E^*$ (keV)
0–20 cm	750	150	150	425
20–40 cm	5000	150	150	800

With these parameters, an improved fit is obtained to the bremsstrahlung spectra, including the narrow emission peak at  $\theta \cong 45^\circ$ . The mean square percent difference between measured and calculated photon emission is reduced to  $\epsilon \approx 25\%$  in this case. It is interesting to note that the calculated  $90^\circ$  emission at 14 keV is almost identical for the homogeneous and the two-step models, and thus the two-step model is also consistent with the radial profile based on 14 keV X-rays viewed at  $90^\circ$ .

The two-step distribution is less energetic in the interior and more energetic on the outside than the homogeneous distribution discussed previously. Fewer energetic electrons ( $> 425 \text{ keV}$ ) in the central region

would mean that the path-length-weighting factors for the higher-energy photon data are too high in the viewing range  $0^\circ < \theta \lesssim 45^\circ$ , thus accounting for the decrease in measured emission for those angles. More radial steps or a smoothly varying  $f(\vec{p})$  with radius might be used to improve the fit. However, a more detailed model with more adjustable parameters is probably not justified in view of the accuracy of the data. The two-step model does indicate that the distribution of higher-energy electrons is weighted toward the outside of the plasma for this particular discharge. The lack of many high-energy electrons ( $> 425 \text{ keV}$ ) in the interior is reasonable since the lower-hybrid wave accessibility condition restricts

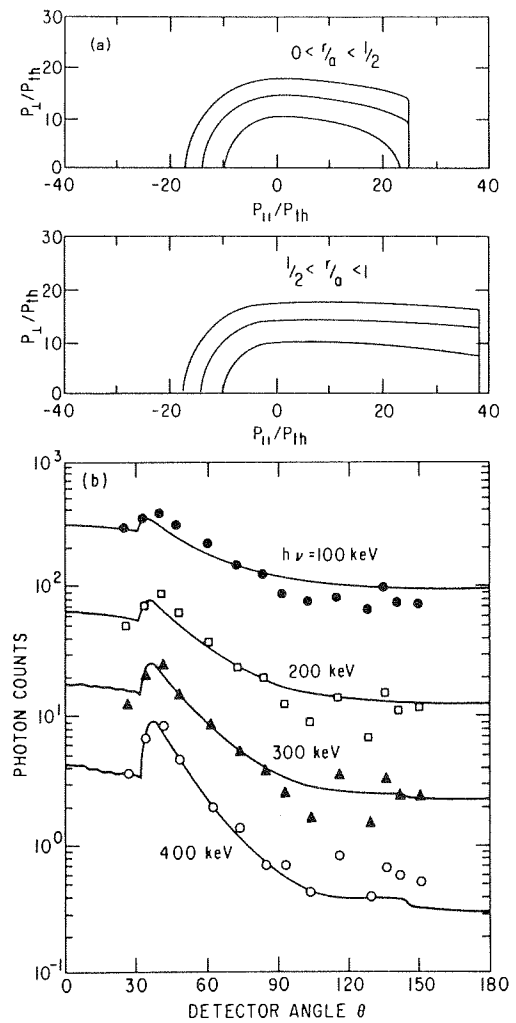


FIG. 8. (a) Two-step radial variation of tail distribution function. Parameters for the two distributions are given in text. (b) Solid lines are bremsstrahlung emission versus  $\theta$  for  $h\nu = 100, 200, 300,$  and  $400 \text{ keV}$ , assuming the two-step distribution shown in (a). Data are same as shown in Fig.2(b).

the phase velocity of the waves capable of penetrating to the interior to approximately 400 keV for the conditions of this particular discharge ( $\bar{n}_e \approx 5 \times 10^{12} \text{ cm}^{-3}$ ,  $B \approx 29 \text{ kG}$ ). It is also reasonable to expect relatively more fast electrons on the outside because faster electrons should diffuse outward before slowing down while slower electrons created in the interior are expected to slow down before having time to diffuse to the outside.

#### 4. COMPARISON OF THE FOKKER-PLANCK SOLUTION WITH THE DATA

A calculation of the electron distribution can be made by using the Fokker-Planck equation with an added quasi-linear term. Details of the background plasma and the RF spectrum must be provided in order to specify the problem completely. In the absence of any definite information about the wave spectrum, the simplest one is chosen, namely [26]:

$$D_{\text{QL}} = D_{\text{RF}} \quad \text{for } W_1 < W < W_2$$

$$= 0 \quad \text{otherwise,}$$

where  $W = v_{\parallel}/v_{te}$  and  $v_{te} = (2kT_e/m_e)^{1/2}$  (note that other papers [25, 26] define  $v_{te} = (kT_e/m_e)^{1/2}$ ). Furthermore, it is assumed that  $D_{\text{RF}} \gg v_{te}^2 \nu_t$ , where  $\nu_t$  is the thermal collision frequency. In that case, the solution to the Fokker-Planck equation is independent of  $D_{\text{RF}}$  and the RF is characterized by just two parameters,  $W_1$  and  $W_2$ . A wide range of realistic spectra may be approximated by this simple form of the equation. To describe the background plasma, an additional dimensionless parameter  $Z_{\text{eff}}$  must be specified. However, since the bremsstrahlung comes primarily from very-high-energy electrons, effects additional to those considered in Ref.[25] must be included. These are relativistic corrections and synchrotron radiation. Since the background temperature is small, the relativistic collision operator reduces to the Landau operator which is easily computed [27]. The synchrotron radiation is calculated in the thin-plasma limit, where it appears as an additional frictional term in the Fokker-Planck equation [28]. The current-carrying tail is again assumed to be homogeneous. The parameters for the background plasma taken from the experimental data are  $n_e = 7.5 \times 10^{12} \text{ cm}^{-3}$ ,  $T_e = 1 \text{ keV}$ , and  $B = 29 \text{ kG}$ . Given these quantities, only the three parameters  $W_1$ ,  $W_2$ , and  $Z_{\text{eff}}$  are left

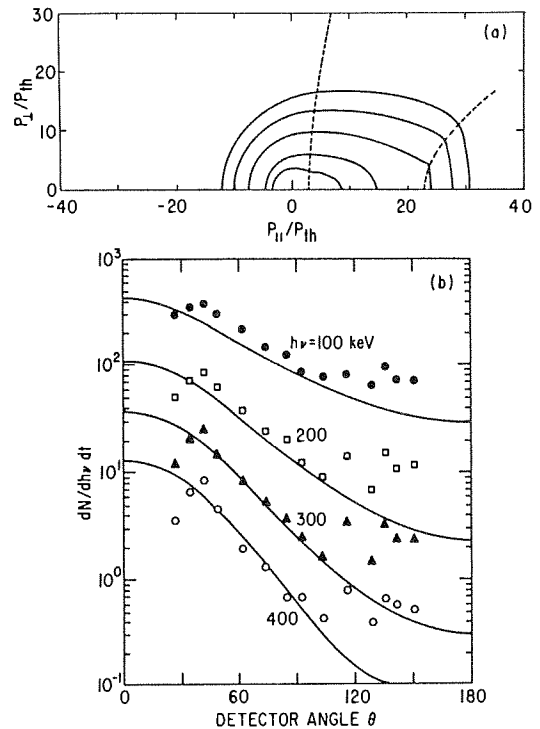


FIG.9. (a) Distribution function calculated from Fokker-Planck theory with large quasi-linear RF diffusion term between  $W_1 = 3$  and  $W_2 = 23$ . 1 keV bulk plasma is assumed for normalization parameter  $p_{\text{th}}$ , and  $Z_{\text{eff}} = 4$ . Every contour represents factor of 2.

(b) Bremsstrahlung emission at  $h\nu = 100, 200, 300,$  and  $400 \text{ keV}$  calculated for distribution in (a). Data are same as shown in Fig.2(b).

to vary. Of these,  $W_1$  is determined by the condition that the current be close to the observed value, giving  $W_1 \approx 3$ . Small changes in  $W_1$  give large changes in the current but only small changes to the bremsstrahlung spectra.

For computational ease, an approximate analytic solution [29] for  $f(\vec{p})$  was used to optimize the fit to the bremsstrahlung data as a function of  $W_2$  and  $Z_{\text{eff}}$ . The best fit occurred in a broad minimum around  $W_2 \approx 20 \pm 4$  and  $Z_{\text{eff}} \approx 4 \pm 2$ . A more exact solution, including relativistic effects and synchrotron radiation, was carried out numerically for  $W_2 = 23$  and  $Z_{\text{eff}} = 4.5$  (Fig.9). The resonance region goes as  $p_{\parallel}/p_{\text{th}} = W_2 (1 + p_{\perp}^2)^{1/2}$  when relativistic effects are included. A contour plot of this solution is shown in Fig.9a, and the calculated bremsstrahlung from this distribution is plotted in Fig.9b along with the data. The fit to the data is quite good considering the simple form of the quasi-linear RF diffusion term that was used. The

main discrepancy between the calculated bremsstrahlung and the data is that not enough emission is predicted for the backward direction ( $\theta \approx 180^\circ$ ).

Consider the values of  $W_1$ ,  $W_2$ , and  $Z_{\text{eff}}$  that are expected in the experiment. The value  $W_2 = 20$  corresponds to a minimum  $n_{\parallel}$  of about 1.28, which is roughly in accord with the expectation of  $n_{\parallel} \cong 1.2$  based on wave accessibility. The value  $Z_{\text{eff}} \cong 4$  agrees with the estimate in Section 5 based on the absolute level of bremsstrahlung emission. The value of  $W_1 = 3$  needed to produce the observed current differs from the expectation of  $W_1 \cong 5.5$  based on the minimum parallel phase velocity of the launched spectrum. This is the 'spectral gap' problem, where the waves are not launched in the range of 3 to  $5.5 v_{te}$  and yet somehow a tail is formed for current drive. Thus, except for this spectral gap, the parameters of the theory which best fit the data have values close to those expected from other considerations.

A number of effects in the experiment are not included in the simplest form of the theory:

- (1) A smaller RF diffusion coefficient ( $D_{QL} < \infty$ ), which would make the forward plateau less flat.
- (2) A weak ( $D_{QL} < 1$ ) spectrum of backward waves which would increase the backward emission.
- (3) Trapped-particle losses which may reduce the perpendicular emission.
- (4) A radial variation in  $f(\vec{p})$ , whose effects were already discussed in Section 3.4.

Various combinations of these effects would produce distributions which better fit the data. However, a complete discussion of the various possibilities will not be attempted here.

In conclusion, a distribution calculated from Fokker-Planck theory with a simple form of the quasi-linear RF diffusion operator gives a good fit to the essential features of the data. This calculation can be used to give an independent estimate for the width of the RF spectrum and the effective ion charge, two parameters which are difficult to measure experimentally.

## 5. DISCUSSION

Knowledge of the electron tail distribution function is important for the following points related to current drive: (1) the number of electrons in the high-energy tail, (2) the energy content of the electron tail, (3) the power dissipated by the tail, (4) the slope of the forward plateau (i.e. wave damping), (5) the  $Z_{\text{eff}}$  of the discharge, and (6) the power radiated by cyclotron

emission and bremsstrahlung. Calculations of the integrated quantities listed above should be used with caution for quantitative predictions because of various uncertainties associated with the model distribution.

The number of tail electrons is computed by assuming that the RF-produced tail carries all the plasma current. The number of tail electrons in the centre of the plasma,  $n_{t0}$ , can thus be derived from the definition of plasma current:

$$I = n_{t0} e \int_0^a 2\pi r \, dr \left\{ \frac{n_t(r)}{n_{t0}} \right\} \int_0^\infty d^3 \vec{p}_0 v_{\parallel} f(r, \vec{p}_0) \quad (7)$$

where  $\{n_t(r)/n_{t0}\}$  is a radial form factor for the current profile based on the soft-X-ray radial profiles, and  $f(r, \vec{p}_0)$  is the normalized distribution function at each radius  $r$ . The assumption that the electron tail carries all the plasma current is reasonable for discharges where the plasma current is constant and where the RF supplies all the external power to the plasma. A central tail density,  $n_{t0}$ , of  $2 \times 10^{11} \text{cm}^{-3}$  is estimated for the discharge which produced the data in Fig.2. This represents approximately 3% of the central electron density.

In principle, the total emission as defined in Eq.(2) can be calculated when  $f(r, \vec{p}_0)$ ,  $n_{t0}$ , and  $Z_{\text{eff}}$  are known. A  $Z_{\text{eff}}$  of approximately 4 gives the observed level of emission for the fit to the data shown in Fig.2, assuming the value of  $n_{t0}$  calculated from expression (7). This value of  $Z_{\text{eff}}$  is unfortunately difficult to check by other means because the present PLT current drive experiments are done in low-density ( $< 10^{13} \text{cm}^{-3}$ ) discharges where plasma resistivity measurements are influenced by superthermal electrons.

The energy content of the electron tail is:

$$E_t = mc^2 e 2\pi R_0 \int_0^\infty 2\pi r dr n_t(r) \int_0^\infty d^3 \vec{p}_0 T_0 f(r, \vec{p}_0) \quad \text{joule} \quad (8)$$

where  $T_0$  is the kinetic energy normalized to  $mc^2$  and  $R_0$  is the major radius. A tail energy content of about 5 kJ is estimated for the discharge which produced the data for Fig.2. This is several times the energy of the bulk electrons measured in similar discharges with TV Thomson scattering. Since the X-ray spectrum from which we deduce  $f(r, \vec{p})$  is primarily determined by the most energetic electrons, the estimate for the total energy content of the tail should be reasonably

accurate. This is not true when calculating power dissipated in the electron bulk by the tail due to collisions [30]:

$$P_D = mc^2 e (3.01 \times 10^{-14}) \ln \Lambda 2\pi R_0 \times \int_0^a 2\pi r dr n_t(r) n_e(r) \int_{p_{\min}}^{\infty} d^3 \vec{p}_0 \frac{E_0}{p_0} f(r, \vec{p}_0) \text{ watt} \quad (9)$$

Here, the major contribution to the velocity space integral comes from tail electrons with  $p \approx p_{\min}$ , where  $p_{\min}$  is the momentum at which the tail distribution meets the bulk distribution. Bremsstrahlung from these low-energy electrons is considerably less than emission from higher-energy electrons; this implies that for low values of  $p$ ,  $f(\vec{p})$  could deviate significantly from the best fit model and drastically change the calculated  $P_D$  without significantly affecting the calculations for  $n_t$  or  $E_t$ . With this strong caution, values of  $P_D \cong 65 \text{ kW} \cong 0.3 P_{\text{RF}}$  are calculated assuming the model in Fig. 2a.

The power radiated at all cyclotron harmonics is calculated from the single-particle emissivity [31]:

$$P_{\text{cyc}} = 2\pi R_0 \int_0^a 2\pi r dr n_t(r) \times \int_0^{\infty} d^3 \vec{p}_0 f(r, \vec{p}_0) \{1.58 \times 10^{-16} B_{\text{kG}}^2 p_{\text{al}}^2\} \text{ watt} \quad (10)$$

A value of  $P_{\text{cyc}} \cong 12 \text{ kW}$  is calculated from the model which is reasonably consistent with the observed values. The power radiated by high-energy bremsstrahlung was found to be negligible:  $P_{\text{BREM}} \cong 20 \text{ W}$ .

The energy confinement time of the high-energy tail is of interest. For example, the whole process of RF current drive depends on confining tail electrons for times longer than the collisional slowing-down time. The energy confinement time for tail electrons is approximately  $\tau_E \cong E_t / (P_{\text{RF}} - P_D - P_{\text{cyc}})$ , where  $P_{\text{RF}} \leq 200 \text{ kW}$  and values of  $E_t \approx 5 \text{ kJ}$ ,  $P_D \approx 65 \text{ kW}$ , and  $P_{\text{cyc}} \approx 12 \text{ kW}$  are derived from the model. This gives  $\tau_E \approx 40 \text{ ms}$ , assuming that all the RF power is absorbed by the tail. Next consider electrons with energies above 200 keV. In this case,  $E_t \approx 4 \text{ kJ}$  from the model distribution and  $P_{\text{RF}} \approx 20 \text{ kW}$  from a

calculation of the grill spectrum (assuming no change in  $n_{\parallel}$  spectrum as the wave propagates). Neglecting  $P_D$  and  $P_{\text{cyc}}$ , which are comparable to  $P_{\text{RF}}$ ,  $\tau_E (mc^2 T_0 > 200 \text{ keV}) \gtrsim 0.1 \text{ s}$ . Even RF spectrum downshifts as large as  $\Delta n_{\parallel} \approx -0.5$ , which are much larger than calculated by ray tracing, do not change this conclusion. Long confinement times for the tail electrons are corroborated by the fact that the power required for current drive depends approximately linearly on the electron density, thus suggesting a collisional slowing-down energy loss mechanism for the tail with  $\tau_E > \tau_s \gtrsim 0.05 \text{ s}$ . In spite of the large uncertainties in the power estimates, it appears that the energy confinement time for 200–600 keV electrons in current-driven discharges is significantly longer than runaway electron confinement times measured previously on PLT [32]. The reason for this difference in confinement is not known. Some possible explanations for the good confinement of the high-energy current-driven electrons are: (1) the much lower density for these discharges, (2) perhaps a lower level of MHD activity ( $q(a) \approx 10$  for the discharge modelled here), and (3) some other confinement property of non-inductively driven discharges. A more quantitative evaluation of the tail ( $mc^2 T_0 > 200 \text{ keV}$ ) energy confinement time is difficult for the method discussed here because it depends inversely on the difference between large, uncertain quantities,  $P_{\text{RF}}$  and  $P_D$ .

Finally, it is desirable to know the slope of the forward plateau in order to estimate the damping of the lower hybrid waves. As was mentioned previously, it is not possible with the present data to distinguish between the case of a relatively flat distribution which is cut off above an energy of  $(E^* - 1)mc^2 = 600 \text{ keV}$  and the case of a smaller forward temperature,  $T_{\parallel F} = 450 \text{ keV}$ , which has no cutoff in energy. Thus, only a lower limit of the  $T_{\parallel F} \gtrsim 450 \text{ keV}$  can be set for the temperature of the forward plateau. In the range of electron energies with which most of the RF power is resonant ( $\lesssim 100 \text{ keV}$ ), the slope of the electron distribution will have only a very small effect on the X-ray spectra. Again, this is because the X-ray spectra are determined primarily by the most energetic electrons. An improvement in accuracy of several orders of magnitude would be required for the bremsstrahlung measurements to be able to give information about the slope of the distribution below 100 keV.

Future measurements may lead to improved models for the tail distribution function. For example, data for angles  $\theta < 28^\circ$  and  $\theta > 152^\circ$  would be useful in determining whether the two-step model, discussed in Section 3.4, is correct. Further experiments that measure the high-

energy bremsstrahlung spectra along different minor radius chords are needed to determine when the distribution  $f(\vec{p})$  varies with minor radius. Such a scan for photon energies up to  $h\nu = 200$  keV and a density of  $\bar{n}_e = 5 \times 10^{13} \text{ cm}^{-3}$  has proved negative on Alcator C [33] while evidence for a radial variation of  $f(\vec{p})$  has been obtained on PLT for certain plasma conditions [9]. Finally, bremsstrahlung measurements at higher energies ( $h\nu > 400$  keV) could make it possible to distinguish whether or not a cutoff energy  $E^*$  exists.

## 6. CONCLUSION

The range of possible electron distribution functions for the lower-hybrid-produced tail has been narrowed significantly by comparing the bremsstrahlung intensity calculated from simple models with the experimental data. Only very anisotropic distributions, with temperatures in the wave direction much higher than perpendicular and backward temperatures, produce calculated bremsstrahlung spectra which fit the main features of the experimental data. In addition, a radial variation of the electron tail distribution function, where the tail on the outside of the plasma is more energetic than on the inside, appears to be able to explain the narrow peak in emission at viewing angles of  $\theta \cong 45^\circ$ . Future experiments should be able to give additional information on key questions such as the radial variation and the maximum energy of the tail.

## ACKNOWLEDGEMENTS

The support of Drs H. Furth, P. Rutherford, and D. Meade is gratefully acknowledged. The authors are indebted to J. Gorman, J. Lehner, and P. Roney for their help with the X-ray diagnostic; J. Lawson and the RF engineering group; and W. Mycock, J. Boychuk, and the PLT technical crew for their many contributions to this experiment.

This work was supported by the US Department of Energy Contract No. DE-AC02-76-CHO-3073.

## REFERENCES

- [1] HOOKE, W., BERNABEI, S., BOYD, D., CAVALLO, A., CHU, T.K., et al., in *Plasma Physics and Controlled Nuclear Fusion Research 1982* (Proc. 9th Int. Conf. Baltimore, 1982), Vol.1, IAEA, Vienna (1983) 239.
- [2] BERNABEI, S., DAUGHNEY, C., EFTHIMION, P., HOOKE, W., HOSEA, J., et al., *Phys. Rev. Lett.* **49** (1982) 1255.
- [3] STEVENS, J., BERNABEI, S., BITTER, M., BOODEY, F., BOWEN, N., CAVALLO, A., et al., in *Heating in Toroidal Plasmas* (Proc. 3rd Joint Grenoble-Varenna Int. Symp. Grenoble, 1982), CEC, Brussels (1982) 455.
- [4] VON GOELER, S., STEVENS, J., KARNEY, C., BERNABEI, S., BITTER, M., et al., in *Radio Frequency Plasma Heating* (Proc. 5th Top. Conf. Madison, 1983) Paper B.2, p.96.
- [5] VON GOELER, S., STEVENS, J., STODIEK, W., BERNABEI, S., BITTER, M., et al., *Course on Diagnostics for Fusion Reactor Conditions*, Vol.1, Varenna, Italy (1982) 87.
- [6] VON GOELER, S., STODIEK, W., in *Controlled Fusion and Plasma Physics* (Proc. 5th Europ. Conf. Grenoble, 1972), Vol.1 (1972) 2.
- [7] VON GOELER, S., STODIEK, W., SAUTHOFF, N., SELBERG, H., in *Toroidal Plasma Confinement* (Proc. 3rd Int. Symp. Garching, 1973) paper B25 (1973).
- [8] KNOEPFEL, H., in *Course on Plasma Diagnostics and Data Acquisition Systems* (EUBANK, H., SINDONI, E., Eds), Editrice Compositori, Bologna (1975).
- [9] VON GOELER, S., STEVENS, J., BERNABEI, S., BITTER, M., CHU, T.K., et al., accompanying paper, this issue, p.1515.
- [10] VON GOELER, S., in *Diagnostics for Fusion Experiments* (SINDONI, E., WHARTON, C., Eds), Pergamon Press, New York (1978).
- [11] ADAMS, F., DAMES, R., *Applied Gamma Spectroscopy* (2nd ed.), Pergamon Press, New York (1970).
- [12] GLUCKSTERN, R.L., HULL, M.H., *Phys. Rev.* **90** (1953) 1030.
- [13] HEITLER, W., *The Quantum Theory of Radiation*, Oxford University Press, London (1954).
- [14] KOCH, H.W., MOTZ, J.W., *Rev. Mod. Phys.* **31** (1959) 920.
- [15] ELWERT, G., *Ann. Phys.* **34** (1939) 178.
- [16] LEE, C.M., KISSEL, L., PRATT, R.H., TSENG, H.K., *Phys. Rev., A* **13** (1976) 1714.
- [17] ELWERT, G., HAUG, E., *Phys. Rev.* **183** (1969) 90.
- [18] TSENG, H.K., PRATT, R.H., LEE, C.M., *Phys. Rev., A* **19** (1979) 187.
- [19] HAUG, E., *Z. Naturforsch.* **30** (1975) 1099.
- [20] HAUG, E., *Z. Naturforsch.* **30a** (1975) 1546.
- [21] BERNHARDI, K., PhD dissertation, University of Bochum, FRG (1980).
- [22] ELWERT, G., *Z. Naturforsch.* **9a** (1954) 637.
- [23] STRATTON, T.F., in *Plasma Diagnostics Techniques* (HUDDLESTONE, R., LEONARD, S., Eds), Academic Press, New York (1965).
- [24] SAUTER, F., *Ann. Phys.* **11** (1931) 454.
- [25] KARNEY, C.F.F., FISCH, N.J., *Phys. Fluids* **22** (1979) 1817.
- [26] FISCH, N.J., *Phys. Rev. Lett.* **41** (1978) 873.
- [27] KARNEY, C.F.F., FISCH, N.J., *Phys. Fluids* **28** (1985) 116.
- [28] BERNSTEIN, I.B., BAXTER, D.C., *Phys. Fluids* **24** (1981) 108.

- [29] FISCH, N.J., KARNEY, C.F.F., Asymptotic Analysis of RF-Heated Collisional Plasma, Princeton Plasma Physics Lab. Rep. PPPL-2205 (1985).
- [30] MOSHER, D., Phys. Fluids 18 (1975) 846.
- [31] BEKEFI, G., Radiation Processes in Plasmas, Wiley, New York (1966).
- [32] BARNES, C., STRACHAN, J., Nucl. Fusion 22 (1982) 1090.
- [33] PORKOLAB, M., SCHUSS, J., LLOYD, B., TAKASE, Y., TEXTOR, S., et al., Phys. Rev. Lett. 53 (1984) 450.

(Manuscript received 12 March 1985  
Final manuscript received 5 August 1985)